

An Automatic Correction Method for the Heel Effect in Digitized Mammography Images

Marcelo Zanchetta do Nascimento,^{1,2} Annie France Frère,^{2,3} and Fernao Germano⁴

The most significant radiation field nonuniformity is the well-known Heel effect. This nonuniform beam effect has a negative influence on the results of computer-aided diagnosis of mammograms, which is frequently used for early cancer detection. This paper presents a method to correct all pixels in the mammography image according to the excess or lack on radiation to which these have been submitted as a result of the this effect. The current simulation method calculates the intensities at all points of the image plane. In the simulated image, the percentage of radiation received by all the points takes the center of the field as reference. In the digitized mammography, the percentages of the optical density of all the pixels of the analyzed image are also calculated. The Heel effect causes a Gaussian distribution around the anode-cathode axis and a logarithmic distribution parallel to this axis. Those characteristic distributions are used to determine the center of the radiation field as well as the cathode-anode axis, allowing for the automatic determination of the correlation between these two sets of data. The measurements obtained with our proposed method differs on average by 2.49 mm in the direction perpendicular to the anode-cathode axis and 2.02 mm parallel to the anode-cathode axis of commercial equipment. The method eliminates around 94% of the Heel effect in the radiological image and the objects will reflect their x-ray absorption. To evaluate this method, experimental data was taken from known objects, but could also be done with clinical and digital images.

KEY WORDS: Heel effect, images processing, computational simulation, x-rays, mammography, digitized film

INTRODUCTION

Radiological diagnosis is based on the analysis of the film optical density differences that should be generated only by the variation of the absorption of the analyzed tissue. Some variations

may be caused by the scattered radiation and intensifying screen blur. Several research groups have worked on the removal of the scattered radiation effects from x-ray images to enhance mammograms.¹⁻³ Blurs from intensifying screens, being a diffusion process, have been extensively modeled and measured to permit image enhancement.⁴ One of the most relevant problems causing field inhomogeneity is the Heel effect and overall nonuniformities in optical densities are correlated with radiation intensity variations.⁵

The tilted x-ray target causes the Heel effect. The x-ray radiation generated in the tilted anode travel along different path lengths undergoing different attenuation causing certain image receptor regions to receive more radiation than others

¹From the Centro de Matemática, Computação e Cognição, Universidade Federal do ABC, Rua Santa Adélia, 166, 09210170, Santo André, SP, Brazil.

²From the Departamento de Engenharia Elétrica, Escola de Engenharia de São Carlos, Universidade de São Paulo, Avenida do Trabalhador Saocarlene, 400, 13560250, São Carlos, SP, Brazil.

³From the Centro de Pesquisas Tecnológicas, Universidade de Mogi das Cruzes, Rua Dr. Cândido Xavier de Almeida Souza, 200, 08780911, Mogi das Cruzes, SP, Brazil.

⁴From the Instituto de Ciências Matemática e de Computação, Universidade de São Paulo, Avenida do Trabalhador Saocarlene, 400, 13560070, São Carlos, SP, Brazil.

Correspondence to: Marcelo Zanchetta do Nascimento, Centro de Matemática, Computação e Cognição, Universidade Federal do ABC, Rua Santa Adélia, 166, 09210170, Santo André, SP, Brazil; tel: +55-11-44371600; fax: +55-11-49963166; e-mail: marcelo.nascimento@ufabc.edu.br

Copyright © 2007 by Society for Imaging Informatics in Medicine

Online publication 11 September 2007

doi: 10.1007/s10278-007-9072-1

leaving them darker. These differences affect the image contrast. Although the intensity inhomogeneity induced by the Heel effect is a smoothly varying function of the position, it is easily corrected by the human visual perception system but complicates the use of automatic processing techniques because the brightness of an object within the image is position-dependent.⁶

Terry et al.⁵ have experimentally investigated the nonuniformity of the x-ray beam itself and they found a decrease of 16% to 40% in the radiation intensity of mammographic equipment along the anode-cathode axis and of 1% to 9% in the direction orthogonal to that axis. For conventional x-ray equipment, Fung and Gilboy have shown that the radiation along the anode-cathode axis suffers a variation of 55% between one and the other end of the radiation field.⁷

Recently, several computational algorithms have been developed and explored for computer-aided detection (CAD) systems to assist in locating and classifying breast abnormalities of digitized mammography images, assuming that they might provide a useful second opinion to radiologist.⁸ However, these algorithms could be prone to errors because of the spatial intensity variations of the applied x-ray field. The application of the corrections against the nonuniform characteristics of acquisition systems before using CAD was described in other papers.^{9,10} In computational vision, the variation in image background density caused by nonuniform illumination is a well-known problem. The majority of the traditional techniques for the correction of nonuniform illumination have been developed for industrial applications, presenting good results. So, their applications in the mammographic CAD systems do not supply satisfactory results, mainly because they do not maintain the correct image densities of the anatomical structures.

In the case of mammograms, Cowen et al.¹¹ coupled a Perspex filter on the x-ray tube window to compensate the Heel effect. They obtained reasonably uniform optical density values for all the field positions. According to the authors, it is necessary to develop a specific filter for each tube.

Highnam et al.,¹² Pawluczyk and Yaffe,¹³ and Behiels et al.⁶ have proposed computational methods to correct the Heel effect in radiological images so that the gray scale variations correspond only to the tissue differences of the analyzed

structure. For this method, Highnam et al.¹² employed a film exposed without object named "black" film, representing the optical densities produced only by the x-ray beam. According to the authors, images with normalized background regions were obtained applying this process on digitized mammograms in the Churchill hospital, in Oxford.

Pawluczyk and Yaffe have described the correction of densities variations produced by the Heel effect in digitized mammograms, combining empirical data with analytical models.¹³ The authors have calculated the incoming radiation intensity at each point of the breast based on the path obliquity, spectral beam hardening, Heel effect, and distance using the inverse-square law. Simulations have been conducted to determine the magnitude of these effects, allowing the gray scales to correspond only to the breast tissue variations. According to the authors, although results obtained with the model have been similar to the experimental results, it does not supply enough precision to exactly compensate all the field variations. A combination between experimental (empirical data) and theoretical (modeling) approaches has allowed the correction of the radiation nonuniformity on multiple radiological systems.

Behiels et al.⁶ proposed a mathematical model that allows the Heel effect to be simulated. With this model, the authors have determined a new image background, calculating a new distribution and correcting the parameters until they converged. The method has provided good results with phantom images and with 137 hand digital radiographs that had a background region sufficiently large to allow the refinement of the parameters of the model. Those methods have provided good results, however, the center position of the radiation field has to be determined experimentally for each system to allow the application of these methods.

In fact, the radiation field generated by an inclined anode is nonisotropic and noninvariant. Therefore, methods simulating the radiological image formation processes need a previous space agreement between the simulated field and the image to be corrected. Pawluczyk and Yaffe obtained this spatial agreement by specific experiments,¹³ and Behiels et al. used successive interactions.⁶

The method that we present allows an automatic correction of the variations caused by the Heel effect without the use of additional reference images and without previous experiments to determine the center of the x-ray field. The radiation center of the field and the anode–cathode axis, to be used in our proposed method, are determined using only on the image to be corrected. The determination of the orientation and localization of the x-ray source is obtained from the digitized radiological image only and is therefore independent of the x-ray equipment and the register system. The corrections of radiological image pixels are made in function of the excess or the lack of radiation that these pixels have been submitted to. Experimental images of known objects were used to validate the proposed method proving that it can be applied on clinical and digital images.

MATERIALS AND METHODS

Image Acquisition

A CGR 500T Senographe radiological unit was used to produce all the test images. The system was equipped with a x-ray tube with a molybdenum anode (Mo), filter Mo, and a beryllium window producing a 0.3-mm nominal sized focus. Although the equipment contains an automatic exposure control system, the parameters were manually adjusted. Five aluminum disks, each with diameter of 10 mm and a thickness of 1.5 mm, were used as phantoms to produce 40 images. Kodak Min-R 2000 and Fuji AD-M films were used to provide high contrast and quality mammograms.¹⁴ The 180×240 mm films were reduced to 140×180 mm maintaining only the regions of interest and were subsequently digitized with a spatial resolution of 169 μ into 8 bits

intensity levels with a VIDAR–Diagnostic Pro equipment providing adequate experimental data.

The exposure techniques and simulations conducted in our experiments are presented in Table 1. To avoid additional noise, a cassette without screen intensifier was used in all our experiments, and therefore, a larger kVp setting was required. This was possible because the kVp has little influence on the Heel effect.

A Mammography Focal Spot Test Stand, manufactured by Nuclear Associates, was used to locate the radiation center of the field through the image obtained by Focal Spot Test Stand Alignment Device (the one bead is centered between the four beads). With this tool, the vertical and horizontal positions of the center of the radiation field were measured with a standard deviation of 0.2 and 0.5 mm, respectively, and used to validate the proposed method.

Radiation Beam Distribution Simulation

To allow the correction of the variations of the optical densities, the radiological image formation process must initially be simulated considering the Heel effect. A user-friendly Delphi programming environment was used to computationally simulate the intensity distribution along the radiation field based on the travel path of the photons inside the target.¹⁵ The correction of the Heel effect was implemented using the continuous slowing-down approximation method (CSDA) as described by Fritz and Livingston.¹⁶

In this method, the radiation spectrum $I_0(E)$ produced by the target for any point of the radiation field was calculated as follows:

$$I_0(E) = CZ(E_0 - E) \left(\frac{v_0}{c^2} \right) \quad (1)$$

where, E is the photon energy, E_0 the electrons emission energy, Z the anode atomic number, v_0

Table 1. Exposure Techniques

Techniques	Parameter				
	KVp	mA	Time (s)	Film	Focus/Image Distance (mm)
T ₁	34	160	1	Fuji AD-M	450
T ₂	34	160	1	Kodak Min-R 2000	450
T ₃	34	200	1	Kodak Min-R 2000	500
T ₄	37	160	1	Fuji AD-M	450

the electron initial velocity, C a constant, and c the velocity of light. The value of constant C was chosen in accordance with the anode material. For molybdenum anode, the value is 0.579×10 .¹¹

Figure 1 shows the x-ray photon emission process. The cathode electrons are attracted by the anode colliding and penetrating in it at high velocities causing the production of internal radiation. During this process, the photons suffer major or minor absorption, depending on their travel path inside the anode. This process is represented in a coordinate system (x , y , and z) (see Fig. 1) with x along the anode–cathode axis, y along the particular direction, and z in the orthogonal direction to that axis. The distance (d) between points A and B of the anode–cathode axis defines the electron penetration depth.¹⁷ Considering (S) the path length of the photons within the target, when emitted toward a point P_2 of the image plane, ϕ the target's inclination angle, θ the angle formed between the emitted ray in the direction of point P_2 and the center of the beam, in other words, between points BC and BD , the path length S to any point of the image plane is given by:¹⁸

$$S(\theta) = \frac{d \cos \phi}{\cos \beta \sin(\phi + \theta)} \quad (2)$$

Equation 3 provides the radiation intensity after passing through the anode material:

$$I(E) = I_0(E) e^{-\mu/\rho \cdot S(\theta)} \quad (3)$$

where, $I(E)$ is the transmitted radiation intensity, $I_0(E)$ is the incident radiation intensity, μ/ρ is the mass attenuation coefficient that depends on the photons incident energy and the target material. Spectrum correction caused by the x-ray tube window and the additional filter must also be calculated. The values used for the mass attenuation coefficients of the materials considered in the simulation in function of photon energies between 1 and 50 keV are given by Boone and Chavez.¹⁹ To get the radiation intensity for all the pixels of the image plane, the spectrum must be integrated in $I(E)$.

In the resultant simulated field, the center of the radiation field, and the anode–cathode axis, as well as the control points every 2 cm along this axis, must be determined. The variation of the radiation intensities must be calculated from each point related to the center of the simulated field.

Determination of the Spatial Correspondence

To determine the spatial correspondence between the simulated field and the radiological image, it is necessary to locate also the projection

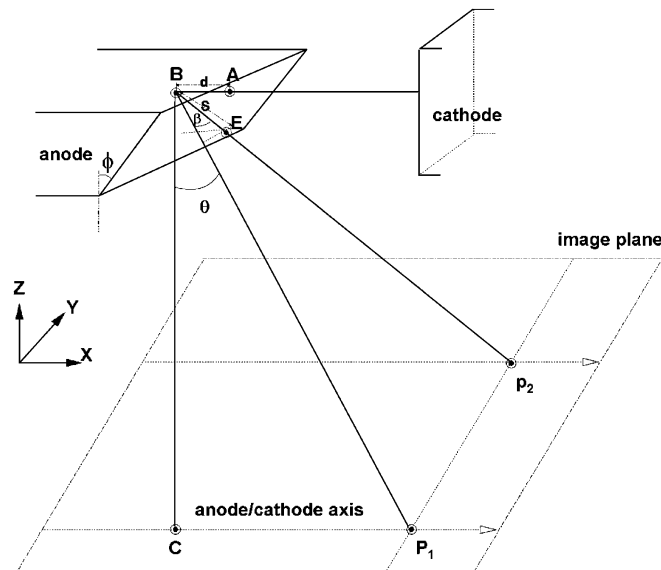


Fig 1. Electron penetration and x-ray photons emission process inside of the target.

of the x-ray tube anode–cathode axis on this image.

One of the Heel effect properties is used to realize the spatial correspondence. Namely, the radiation field intensities are symmetrically distributed in the perpendicular direction of the anode–cathode axis as shown in Figure 2a. Using this feature, the position of the anode–cathode axis can be obtained from the distribution simulation. To determine the similarity of pixels between the S_1 and S_2 region, an area without object information must be found in the radiological image (see Fig. 2a). The Sobel edge detector²⁰ and the Otsu threshold algorithm were applied to locate this area and two bands A and B must be analyzed (see Fig. 2b). A second degree polynomial regression, based on the least square methods along with the application of the median filter derived by simply choosing the “median” pixel in the 3×3 pixel neighborhood, are used to reduce the quantum noise of these bands.²¹ The similarity of the pixels densities of each band within the S_1 and S_2 area is examined until finding those that present a high percentage of similarity of its gray scales densities.

Half of the M_1 distance, between the pixels pair with maximum similarity of band A , determines the location of one point of the projection of the anode–cathode axis.

The same method is applied in band B , finding M_2 . The projection of the anode–cathode axis in the image passes through M_1 and M_2 .

A *B-spline* interpolation function is applied on the density values of the anode–cathode axis projection:

$$P(t) = \sum_{i=0}^n N_{i,k}(t)p_i \quad (4)$$

where p_i ($i=0, \dots, m$) are the control points, k is the degree, and n is the number of points of the final polygon. The $N_{i,k}$ functions are given by the following recursive formula, known as the Cox-de Boor algorithm:²²

$$N_{0,k}(t) = \begin{cases} 1 & \text{if } t_i \leq t < t_{i+1}, \\ 0 & \text{otherwise} \end{cases}$$

$$N_{i,k}(t) = \frac{(t-t_i)}{t_{i+k}-t_i} N_{i,k-1}(t) + \frac{(t_{i+k+1}-t)}{t_{i+k+1}-t_{i+1}} N_{i+1,k-1}(t) \quad (5)$$

where $t_0 \leq t_1 \leq \dots \leq t_{n+k}$ are the parameterization knots.

In the radiological image, the control points must be determined so that the percentage variation of their gray scales is equivalent to the radiation intensity variations found in the simulated field. Because in our case the used densities are collected in the linear region of the HD curve of the film, we can consider that the densities' variations will correspond to the radiation intensity variations.

Figure 3 shows selected points in the anode–cathode axis of the radiological image and those of the simulated field. A 3×3 -pixel neighborhood on

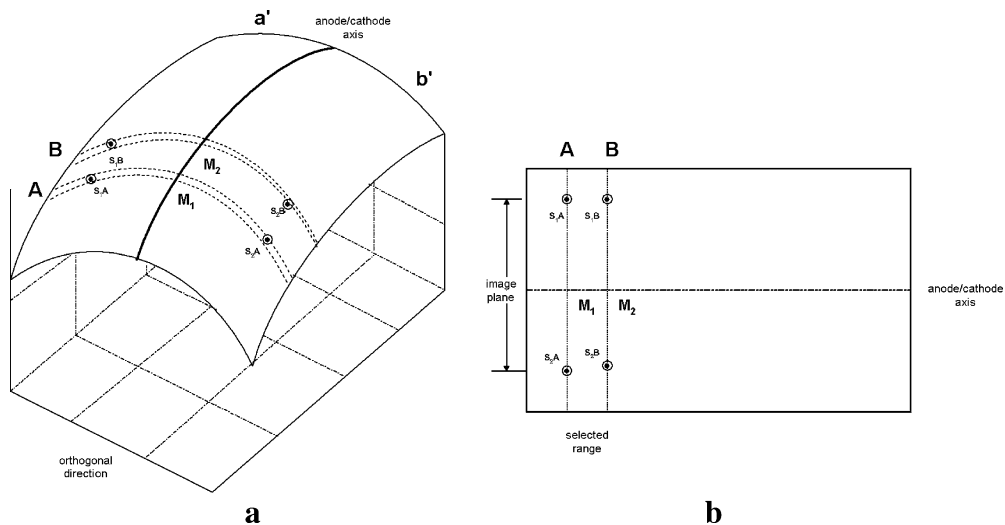


Fig 2. a Distribution of the densities in a direction perpendicular to the anode–cathode axis. b Divisions of the image for the determination of the anode–cathode axis.

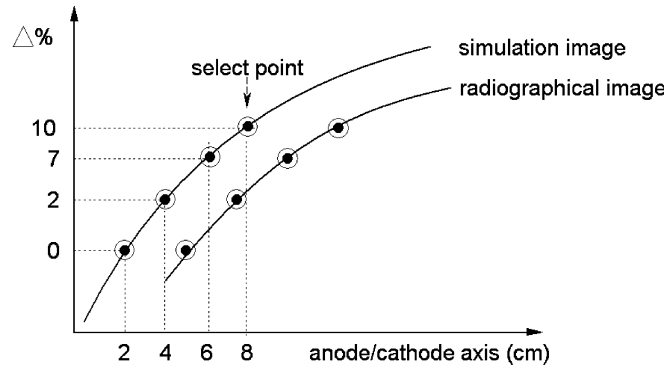


Fig 3. Selection of points of control in the anode–cathode axis of the simulation and radiological image.

each control point is used to measure the similarity between the values of the two analyzed sets (Eq. 6):²³

$$r = \frac{\sum_{i=1}^n x_i y_i - \frac{1}{n} \left(\sum_{i=1}^n x_i \right) \left(\sum_{i=1}^n y_i \right)}{\sqrt{\left(\sum_{i=1}^n x_i^2 - \frac{1}{n} \left(\sum_{i=1}^n x_i \right)^2 \right) \left(\sum_{i=1}^n y_i^2 - \frac{1}{n} \left(\sum_{i=1}^n y_i \right)^2 \right)}} \quad (6)$$

where x_i is the gray scales densities of the i pixel in the radiological image, y_i is the gray scales densities of the i pixel in the simulated field, and n is the analyzed pixels number in the 3×3 -pixel neighborhood.

To analyze the correspondence between the radiological image pixels and the points of the simulated field, a polynomial mapping function based on least squares techniques is applied. The control points of the two images are overlapped to allow the localization of the center of the field of the radiological image.

Heel Effect Correction

To correct the density variations caused by the Heel effect, the percentages of radiation received by each pixel from the simulated image in relation to the center of the field must be calculated. These percentages are stored in a matrix of pixels named “background image”.

The variation in percentage of the density of each pixel of the radiological image regarding the density of the center of the field is calculated and is store in a “radiological image” matrix.

The final “corrected image” matrix is obtained subtracting the “background image” matrix from the “radiological image” matrix.

This new image registers only the variation percentages caused by the radiological structures. These values are converted into gray scale densities, considering as reference the density of the center of the field of the radiological image.

RESULTS

Figure 4 shows the digitized image of the five equal phantoms obtained with the exposure condition E_1 . An arrow point marks the experimentally obtained center. Figure 4b shows the influence of the Heel effect on this radiological image in 3-D where we can observe that the contrast of each object is different and depends on its position in the radiation field.

Figure 5 presents the gray scale average values of bands A and B of the radiological image reduced to lines obtained with technique E_1 .

Table 2 presents the correlation between the simulated field control points and the radiological image obtained with the exposure condition E_1 together with the correlation percentage.

Figure 6 shows the obtained localization of the anode–cathode axis and the center of the field on top of the Figure 4a. The white line indicates the projection of the anode–cathode axis. Its intersection with the perpendicular line indicates the calculated center of the field, whereas the white arrow indicates the experimentally defined position.

Table 3 presents the largest error for localization of the center measured with the commercial

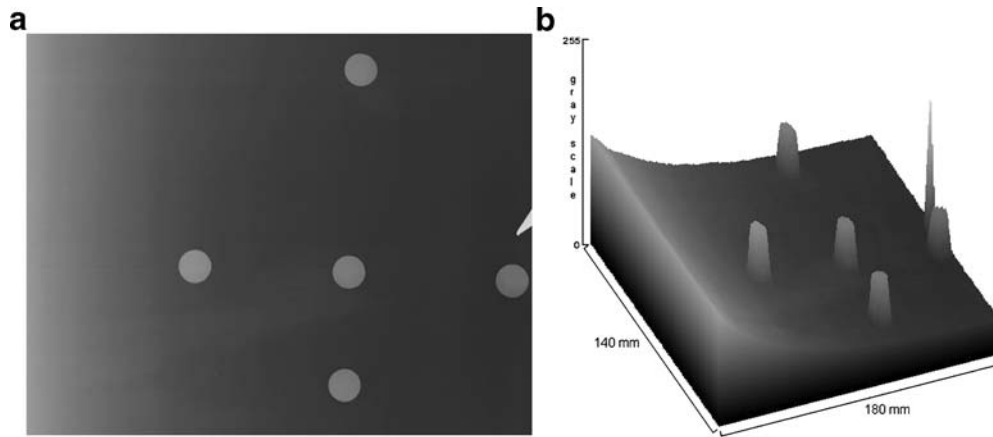


Fig 4. a Digitalized radiographic image obtained with 34 kVp, 160 mA, and 1 s. b Three-dimensional representation of the gray scale distribution of a.

equipment; those calculated with our method and the difference in each of the exposure techniques. The signal placed before the deviation value indicates if the localization of the calculated center is before (-) or after (+) the measured position with the commercial equipment, X indicates the direction perpendicular to the anode-cathode axis and Y indicates the direction parallel to the axis.

After simulating the virtual image and calculating the density variations in relation to the center, the densities of the radiological image were corrected in function of this simulation. Figure 7a shows the results obtained after applying the algorithm for correction of the Heel effect on the image of Figure 4a. A 3-D presentation of the corrected gray

scale intensities were shown in Figure 7b. The three-dimensional representation of the density distribution of the image shows that the algorithm has also correctly reconstructed the densities of the phantoms.

The density values used to determine the center of the field in the anode-cathode direction are presented in Figure 8a where Figure 4a shows the values before the correction and Figure 7a after the applied method. In Figure 8b, the same representation is presented perpendicular to the anode-cathode direction.

To evaluate the correction, we show in Table 4 the standard deviation σ of the estimated background of all images produced by the four

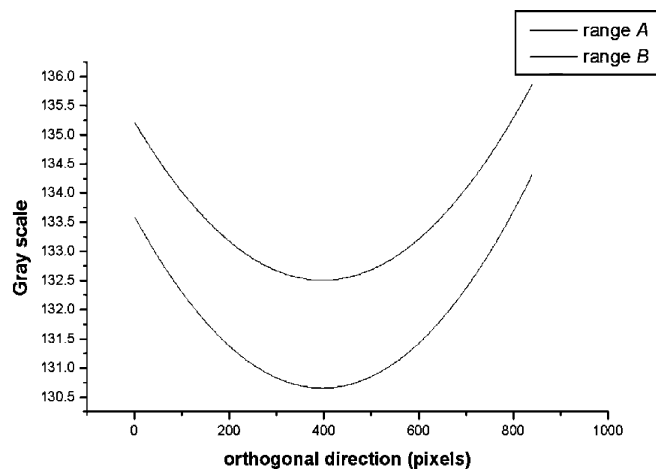


Fig 5. Graphic representation of selected line average in bands A and B for the determination of the anode-cathode axis in the image of Figure 4a.

Table 2. Correlation Between the Simulated Field Control Points and the Radiological Image, Together with the Correlation Percentage

Point of Control	Correlation	Percentage
1	0.887	89
2	0.844	84
3	0.846	85
4	0.886	89
5	0.869	87
6	0.873	87
7	0.951	95
8	0.984	98
9	0.966	97

exposition techniques before and after the application of our correction method as well as the removed noise.⁶

DISCUSSION

To evaluate the proposed method, various data acquisition conditions were changed. The presented results show that the developed algorithm can efficiently determine the anode–cathode axis in all cases. The localization of the anode–cathode

axis was evaluated with a correlation function. This correlation function permits the generation of a metric to compare the similarity between the simulated and the mammographic images. An average similarity of about 90% was obtained. This value is considered satisfactory by Dekker et al.²⁴ in his evaluation of radiotherapy images.

The largest error with the proposed method used to define the position of the radiation center of the field parallel to the anode–cathode axis, even when it was compared to the measured position obtained with the commercial equipment, was 3.38 mm of the 180-mm analyzed region of interest. In the perpendicular direction, the largest observed error was 3.89 mm of the 140-mm region of interest. However, the method differs on average by 2.49 mm (1.78% of the image) in the direction perpendicular to the anode–cathode axis and 2.02 mm (1.12% of the image) parallel to the axis.

The small differences between the obtained results of the two methods can be attributed to: quantum noise, digitalization, and processing inaccuracies. The influence of these errors on the performance of the method was also analyzed. Three-dimensional representations of the pixel density distributions of the corrected images

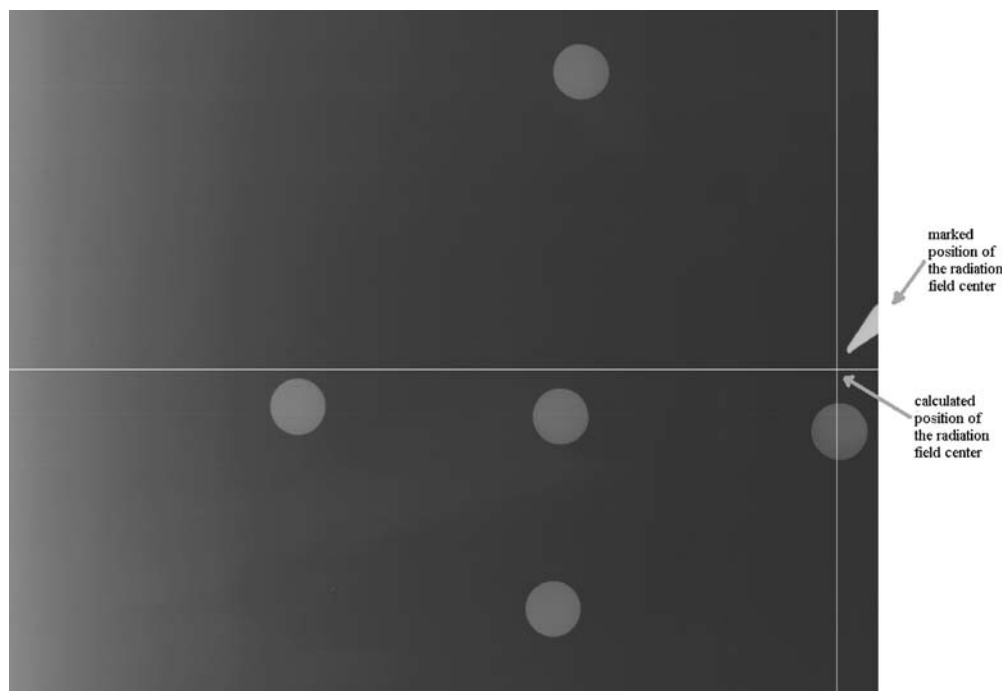


Fig 6. Localization of the field center in the digitized radiological image obtained with 34 kVp, 160 mA, and 1 s.

Table 3. Localization of the Center Measured with the Commercial Equipment and Calculated with our Method and their Deviation (Pixel Size 0.169 mm)

Exposure	Measured with Commercial Equipment		Calculated with Method		Deviation Error (in Pixels)		Percentage	
	X	Y	X	Y	X	Y	X	Y
E ₁	937	425	925	431	-12	+6	-1.28	1.41
E ₂	935	353	929	330	-6	-23	-0.64	-6.52
E ₃	1,024	355	1,004	333	-20	-20	-1.95	-5.63
E ₄	1,009	412	1,015	402	+6	-10	0.59	-2.43

indicates that the method is capable of obtaining uniform background regions, maintaining the contrast of the objects, obtaining better results than those presented by majority of the traditional techniques for the correction of nonuniform illumination.

A quantitative study of the density variations of the background of the images shows that our method was also efficient in removing background noise; capable of reducing the noise to an average of 94.55%.

CONCLUSION

The variations of the contrast between radiographic objects and background image along the cathode–anode axis has been corrected, and the obtained densities of the objects are now only determined by their absorption characteristics. This was possible as our method was based on the simulation of the physical process involved in the radiological image generation including the

characteristics of the used x-ray beam. As the method was developed considering the physical behavior of the x-ray, generation could also be used in digital radiography.

The correction was automatic and independent of the position of the image receiver; no previous or additional measurement to localize the center of the field were needed. This fact makes our procedure much easier compared to the technique proposed by Highnam et al.¹² and Pawluczyk and Yaffe,¹³ in which the position of the recording device in relation to the x-ray source must be marked in each image. Several experimental devices were described in the literature to determine the position of the x-ray source in relation to the image receiver. However, important factors restrict the use of such devices: time, materials, and a trained operator. The method presented in this paper provides a precise space agreement between the simulated image and the image to be corrected.

In all the tests conducted, the largest error obtained to determine the projection of the center

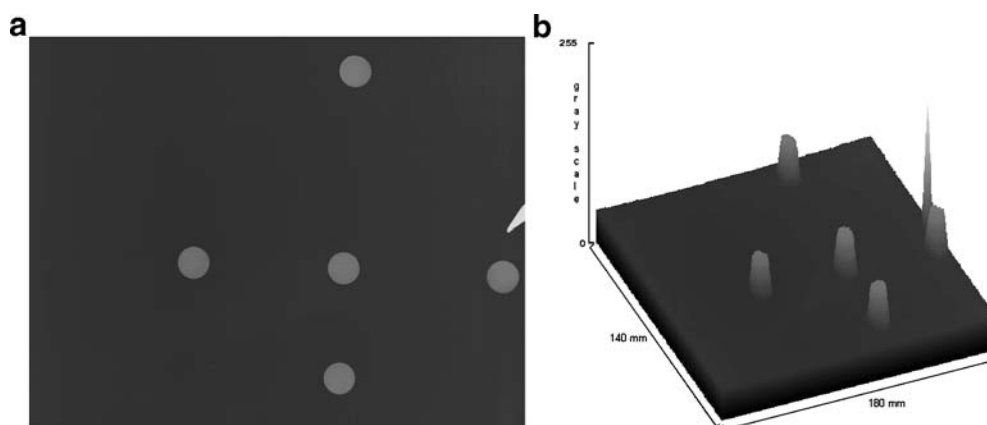


Fig 7. a Image obtained after the algorithm for correction of the heel effect. **b** Graph with 3-D representation of the gray scale distribution of the corrected image.

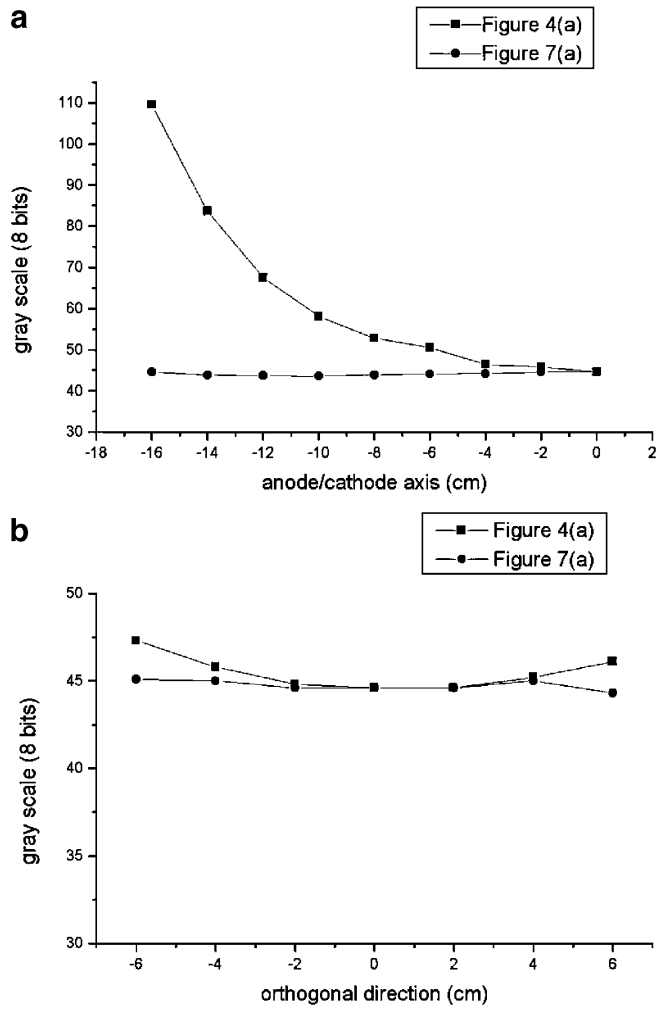


Fig 8. Gray scale obtained before (Fig. 4a) and after (Fig. 7a) the algorithm applied in the image of Figure 4a. a Direction parallel to the anode–cathode axis. b Direction perpendicular to the anode–cathode axis.

of the radiation field regarding those obtained with commercial equipment was within 3.89 mm (2.78% of the image) of the image in the direction perpendicular to the anode–cathode axis and 3.38 (1.88% of the image) in the parallel direction. This small deviation occurs probably because of the quantum noise, digitalization, and processing influences.

The method developed to cancel the Heel effect not only allowed the densities of all pixels in the image background to be approximately constant (maximum average variation of 5.45%), but also reduced the image background noise to more than 93%.

Other image processing techniques capable of correcting nonuniform backgrounds in CAD sys-

tems can be found in literature, but in most cases, these methods do not use models describing the origin of the distortions. These techniques are not developed considering the physical behavior of the x-ray generation and consequently fail to remove

Table 4. Standard Deviation Obtained, σ , After Application of the Algorithm Considered of the Difference of the Average Value of the Intensity of Background for the Images

Exposure	Original	Proposed Method	% ^a
E ₁	22.86	0.63	97.25
E ₂	11.57	0.77	93.35
E ₃	10.81	0.60	94.44
E ₄	19.30	1.32	93.16

^aPercentage of the removed standard deviation for the considered method.

the noise in mammograms without affecting small structures relevant for clinical diagnosis. In future researches, we will apply our automatic Heel effect correction method as a preprocessing tool on digitized mammograms and expect to obtain better CAD diagnoses.

ACKNOWLEDGMENTS

The authors wish to express their appreciation for the financial support of FAPESP (Fundação de Amparo à Pesquisa do Estado de São Paulo).

REFERENCES

1. Rezentes PS, de Almeida A, Barnes GT: Mammography grid performance. *Radiology* 210:227–232, 1999
2. Kimme-Smith C, Sayre J, McCombs M, Gold RH, Basset LW: Mammography fixed grid versus reciprocating grid: evaluation using cadaveric breasts as test objects. *Med Phys* 23:141–147, 1996
3. Seibert JA, Boone JM: X-ray scatter removal by deconvolution. *Med Phys* 15:567–575, 1988
4. Highnam R, Brady M, English R: Detecting film-screen artifacts in mammography using a model-based approach. *IEEE Trans Med Imag* 18:1016–1024, 1999
5. Terry JA, Waggner RG, Blough MA: Half-value and intensity variations as a function of position in the radiation field for film-screen mammography. *Med Phys* 26:259–266, 1999
6. Behiels G, Maes F, Vandermeulen D, Suetens P: Retrospective correction of the heel effect in hand radiographs. *Med Image Anal* 6:183–190, 2002
7. Fung KKL, Gilboy WB: “Anode heel effect” on patient dose in lumbar spine radiography. *Br J Radiol* 73:531–536, 2000
8. Rangayyan RM, Ayres FJ, Desautels JEL: A review of computer-aided diagnosis of breast cancer: toward the detection of subtle signs. *J Franklin Inst* 344:312–348, 2007
9. Ferrari RJ, Rangayyan RM, Desautels JEL, Borges RA, Frere AF: Identification of the breast boundary in mammograms using active contour models. *Med Biol Eng Comput* 42: 201–208, 2004
10. Nakayama R, Watanabe R, Namba K, Takeda K, Yamamoto K, Katsuragawa S, Doi K: Computer-aided diagnosis scheme for identifying histological classification of clustered microcalcifications by use of follow-up magnification mammograms. *Acad Radiol* 13:1219–1228, 2006
11. Cowen AR, Brettle DS, Workman A: Technical note: Compensation for field non-uniformity on a mammographic X-ray unit. *Br J Radiol* 66:150–154, 1993
12. Highnam R, Brady M, Shepstone B: A representation for mammographic image processing. *Med Image Anal* 1:1–18, 1996
13. Pawluczyk O, Yaffe MJ: Field nonuniformity correction for quantitative analysis of digitized mammograms. *Med Phys* 28:438–444, 2001
14. Meeson S, Young KC, Rust A, Wallis MG, Cooke J, Ramsdale ML: Implications of using high contrast mammography X-ray film-screen combinations. *Br J Radiol* 74:825–835, 2001
15. Marques MA, Frère AF, Oliveira HJQ, Azevedo-Marques PM, Schiabel H: Computerized method for radiologic systems parameters simulation intended to quality assurance programs. *Med Biol Eng Comput* 37:1244–1245, 1999
16. Fritz SL, Livingston WH: A comparison of computed and measured heel effect for various target angles. *Med Phys* 9:216–219, 1982
17. Brice DK: Stopping Powers for Electrons and Positrons, ICRU Report 37. Bethesda, MD: International Commission On Radiation Units And Measurements, 1984
18. Silva MA, Frère AF, Marques MA, Mattos LS: Heel effect’s influence on the performance of screen-film combinations. *Med Biol Eng Comput* 37:1258–1259, 1999
19. Boone JM, Chavez AE: Comparison of x-ray sections for diagnostic and therapeutic medical physics. *Med Phys* 23:1997–2005, 1996
20. Gonzalez RC, Woods RE: *Digital Image Processing*, 2nd edition. Englewood Cliffs, NJ: Prentice Hall, 2002
21. Press WH, Teukolsky SA, Vetterling WT, Flannery BP: *Numerical Recipes in C. The Art of Scientific Computing*, 2nd edition. Cambridge: Cambridge University Press, 1992
22. Lengyel E: *Mathematics for 3D Games Programming and Computer Graphics*, 2nd edition. Devon, UK: Charles River Media, 2003
23. Pratt WK: Correlation techniques of image registration. *IEEE Trans Aerosp Electron Syst* 10:353–358, 1974
24. Dekker N, Ploeger LS, Herk MV: Evaluation of cost functions for gray value matching of two-dimensional image in radiotherapy. *Med Phys* 30:778–784, 2003